Microchemical Journal 139 (2018) 139–149

Contents lists available at ScienceDirect

Microchemical Journal

journal homepage: www.elsevier.com/locate/microc

Multivariate cathodic square wave stripping voltammetry optimization for nitro group compounds determination using antimony film electrodes

Jessica Moreno Betancourth, Mariela Cuellar, Patricia I. Ortiz, Valeria Pfaffen *

INFIQC–CONICET and Universidad Nacional de Córdoba. Ciudad Universitaria, 5000 Córdoba, Argentina

ARTICLE INFO

Article history:
Received 21 December 2017
Received in revised form 20 February 2018
Accepted 21 February 2018
Available online 24 February 2018

Keywords:
Antimony film electrode
Response surface methodology
Desirability function
4,6-Dinitro-o-cresol

ABSTRACT

The main goal of this paper is the optimization of the square wave voltammetric response of antimony film electrode (SbFE) to determine reducible nitro groups using response surface methodology (RSM). The SbFE was prepared on a glassy carbon electrode (GCE) while cathodic stripping square wave voltammetry (CSSWV) was used as detection technique. In this study, the optimization process of solution pH and 4,6-dinitro-o-cresol (DNOC) accumulation time was carried out using a Central Composite Design (CCD) while a Box–Behnken Design for SWV instrumental variables optimization. The two reduction current peaks were used as dependent variable to evaluate the performance of the system. For solution pH and DNOC accumulation time the optimization process considered only reduction current peak, while for SWV instrumental parameters (step, amplitude and frequency) both the relationship between current peak and standard deviation with the different factors were analysed, finally both designs were quantitatively described by a multivariate regression model through the RSM. Furthermore, the optimal parameter combinations were obtained by maximizing the reduction current peak and minimizing standard deviation within the studied experimental range. Under the optimal parameter combination, a linear calibration curve ranged from (1.0 to 15) $\times 10^{-6}$ mol L^{-1} with a detection limit of 1.12×10^{-6} mol L^{-1} was obtained. The proposed analytical procedure was further applied to detect DNOC in natural water samples with satisfactory results.

1. Introduction

Among different electrochemical techniques, stripping voltammetry plays an important role and has long been recognized as one of the most powerful tool in trace and ultratrace analysis of heavy metals and some organic compounds, due to its exceptional sensitivity in conjunction with different electrode materials [1]. Moreover, electrochemical methods are known for their relative simplicity, low-cost instrumentation and possibility of system integration and miniaturization. Therefore, on-site testing can be carried out, such as environmental monitoring, industrial control and measurements in specific and more challenging environments, e.g. in vivo studies. It is well known that a proper choice of the electrode materials is a crucial factor in assuring a favourable performance of a stripping voltammetric procedure.

The search for new electrode materials and sensors surfaces is systematically pursued in modern electroanalytical chemistry. For decades mercury electrodes has been providing the best characteristics for application in electrochemical analysis of metals and some reducible organic compounds. In recent years the use of mercury-based electrodes has been decreasing due to their toxicity and handling problems. Search for new electrode materials or modifications of currently used materials possibly replacing mercury electrodes and applicable for metallic and organic analytes resulted in the introduction of antimony film electrodes (SbFEs) [2]. In a relatively short time, these electrodes have attracted much attention, which is reflected in the growing number of special studies focused on the SbFEs [3]. This electrode was employed successfully in electrochemical stripping analysis to determine metals [4–21]. However, as far as we know there were only a few works that use it for organic compounds i.e. sulfasalazine [22], pantoprazole [23], food dyes allura red with tartrazine [24], tetracyclines [25], and trifluralin [26]. Trifluralin belongs to the class of so called dinitroaniline herbicides and as the name suggests, it contains two nitro groups on a benzene moiety. Both these groups are electrochemically reducible via simultaneous 8-electron reduction to hydroxylamine groups in acidic medium [27–29]. In these studies, authors focused on the characterization and the comparison of different substrate electrode materials used for the preparation of antimony film electrodes and concluded that the antimony film glassy carbon electrode provide the best results. Nevertheless, the field of analytical optimization of nitro groups electroanalysis based on the antimony electrode has still remained completely unexplored and certainly needs a particular attention. Therefore, further

* Corresponding author.
E-mail address: mpfaffen@fcq.unc.edu.ar (V. Pfaffen).

https://doi.org/10.1016/j.microc.2018.02.028
0026-265X/

investigation of SbFEs for the determination of organic compounds using another pesticide with two nitro groups (4,6-dinitro-o-cresol) as a model compound is presented in this paper.

4,6-dinitro-o-cresol (DNOC) is used agriculturally as a larvicide, ovicide and insecticide (against locusts and other insects) as well as a potato haulm desiccant. It is also used as a polymerization inhibitor and as an intermediate in the chemical industry. For agricultural uses, DNOC is mainly formulated as emulsifiable concentrate, either aqueous or oily [30]. The main sources of human exposure are from contact during manufacturing, and from use in agriculture and in the plastics industry. Because of the known acute toxicity and the strong yellow staining of the skin, agricultural workers are careful to use adequate protective clothing in order to reduce dermal exposure. In the plastics industry, DNOC is made and transported as a powder often dampened with water (12% by weight) to reduce the risk of workers' exposure to dusts. DNOC has caused acute poisoning in humans with several symptoms. Effects are enhanced at high environmental temperature. These effects are consistent with the proposed mechanism of action of DNOC. For these reasons it is important to have fast and sensitive methods for DNOC determination.

In order to identify the best variables operating conditions, the response surface methodology as Central Composite or Box–Behnken designs [31] is commonly and usefully used. These methods allow the simultaneous analysis of more than one factor at the same time and their statistical significance to reduce the number of experiments, minimize reagent consumption, and assess the interaction between the factors. A proper design matrix can lead to a regression equation which highlights effects of individual factors and their relative importance in a given operation process. The possibility of evaluating the interaction effects between the variables on the response can also be used, that is not possible in a classical method (one-factor at-a-time (OFAT)) [31]. If the factors are independent (which is rarely the situation), the most common practice is OFAT while holding all others parameters constant. However, the result of this univariate analysis shows inadequate optimization toward response(s). Moreover, OFAT approach is costly in sense of time and reagents. There is now increasing recognition that hereditary malpractice ought to be replaced by soundly based reliable methods, such as response surface methodology (RSM) based on statistical design of experiments (DOEs). Until now, few reports of the voltammetric response optimization using response surface methodology (RSM) have been published [25,32–36]. Nevertheless, there is lack of articles on the voltammetric response optimization for modified electrode in DNOC determination using RSM.

This study has been focused on the multivariate optimization of chemical and cathodic stripping square wave voltammetry (CSSWV) instrumental variables by RSM to determine the pesticide DNOC as model of nitro group compounds. The SbFE has been prepared on a glassy carbon electrode and CSSWV has been used for DNOC determination in water samples. Applicability of this method has been verified by DNOC quantification in natural water samples.

2. Material and methods

2.1. Apparatus

Square wave voltammetry and potentiostatic measurements were all performed with Autolab (PGSTAT 101 Eco-Chemie) potentiostat controlled by NOVA software (Eco Chemie). A conventional three-electrode system was used where glassy carbon (GCE, 3 mm 75 diameter), a platinum wire, and a Ag/AgCl (3 M KCl) were used as working, auxiliary, and reference electrodes, respectively. All potentials are referred to this reference electrode. All electrochemical experiments were carried on at room temperature. Test solutions were stirred during DNOC deposition and cleaning steps with a magnetic stirrer.

2.2. Reagents and solutions

All reagents were obtained as analytical grade and used without further purification. Milli-Q water obtained from a purifying system (18 Mcm^{-1}) Millipore was used for all experiments. 4,6-Dinitro-o-cresol (DNOC) and $SbCl_3$ were purchased from Sigma–Aldrich (St. Louis, MS, USA). Phosphoric acid, acetic acid, sodium acetate, boric acid, hydrochloric acid, and potassium hydroxide were from J.T. Baker. Britton Robinson buffer solution (BRBS) with different pH values was prepared by mixing acetic acid, phosphoric acid, and boric acid to a final 0.12 mol L^{-1} concentration of each component and the pH was adjusted to the required value by adding either 1.0 mol L^{-1} hydrochloric acid (HCl) or potassium hydroxide (KOH) solution. The 1×10^{-3} mol L^{-1} $SbCl_3$ stock solution was prepared by dissolving the appropriate amount of the solid salt in diluted 5% HCl solution. The electrodeposition solution (5×10^{-5} mol L^{-1}) was prepared in a 10 mL volumetric flask by adding 0.50 mL of stock solution and diluting to 10 mL with acetic buffer solution pH 4.50. To evaluate the accuracy and applicability of the proposed method, the optimized procedure for different water samples was performed. Water samples were taken from different sources, San Roque Lake, Rio Tercero River and drinking water from Córdoba city local net, all locations from Córdoba, Argentina. The collected water samples were filtered through a 0.45 μm Micropore membrane and maintained in glass containers, then stored at 4 °C until they were analysed. For each sample, a 2.0 mL aliquot was transferred to a 10 mL calibration flask, and then DNOC standard solution was added to a 5×10^{-6} mol L^{-1} final concentration and filled with buffer solution.

2.3. Preparation of SbFE

The glassy carbon electrode was mechanically polished with 0.05 μm alumina/water slurry (Buehler, USA) on a polishing cloth to a mirror-like finish, followed by a sonication step, rinsed with distilled water, dried in air and inserted into the electrochemical cell. The antimony film electrodeposition was carried out at a constant potential in the electrodeposition solution by applying a −1.00 V deposition potential for 60 s. To remove the bismuth film, a potential step of +0.5 V for 60 s in BRBS was applied, after which a fresh film deposition was performed.

2.4. Experimental procedure

The determination of pesticides such as DNOC (Scheme 1) can be carried out by a cathodic electrochemical process, corresponding to the nitro group reduction as proposed in the literature [27–29]. In this work, DNOC determinations were done by cathodic stripping square wave voltammetry (CSSWV) with a previous accumulation step, and two peaks were obtained. The SWV parameters together with the

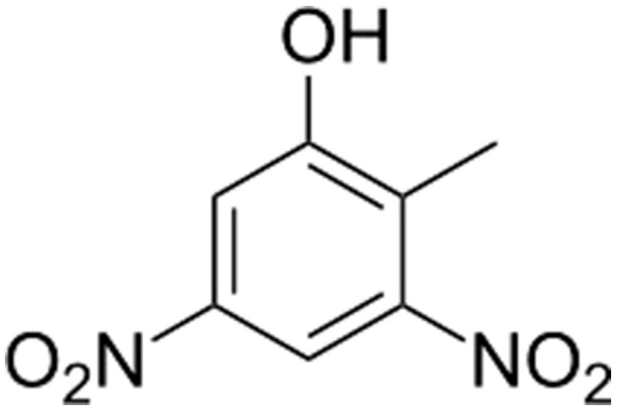

Scheme 1. 4,6-Dinitro-o-cresol (DNOC) structure.

solution pH and the accumulation time were evaluated by factorial designs. The following optimized SWV procedure was used: 10 mL of DNOC solution in 0.12 mol L^{-1} BRBS pH 2.0 were transferred to the voltammetric cell and deaerated by bubbling oxygen-free nitrogen for 5 min; the nitrogen stream was then kept over the solution. After equilibrium time (5 s), a square wave cathodic potential scan was applied between −0.2 to −1.0 V vs. Ag/AgCl (3.0 mol L^{-1} KCl) with the following settings: frequency 120 Hz, amplitude 0.10 V and step potential 0.01 V. All measurements were carried out three times with the same SbFE (n = 3) for each concentration.

2.5. Data analysis

Experimental designs, statistical analyses, and regression models were performed by Design-Expert 7.0.0 software. The adequacy of the developed models was tested by the analysis on R-squared (R^2), adjusted R-squared (R^2_{adj}) and predicted R-squared (R^2_{pre}), and its statistical significance was checked by a Fisher F-test. The level of significance was given as values of the probability <0.05

2.6. Experimental design

RSM is an empirical statistical technique employed for multiple regression analysis by using quantitative data. This method varies the different variables simultaneously and obtains a multivariable equation from properly designed experiments. The graphical representation of their functions is called response surface, which is used to describe the individual and interaction effects of the test variables and their interaction effect on the response [31,37]. The CCD was proposed for the analysis of two factors, as BBD can be used only for three or more factors. The BBD was specifically selected when three or more factors are considered since it requires fewer runs than CCD [31].

According to CCD and BBD matrix design (Tables 1 and 2) to predict the mathematical relationship between independent factors and the dependent response, a second order polynomial model must be fitted to experimental results. During optimization process, relationship of response, main variables, and interactions can be formulated as a quadratic model which also includes the linear terms:

$$Y = \beta_0 + \sum_{i=1}^{k} \beta_i x_i + \sum_{i=1}^{k} \beta_{ii} x_i^2 + \sum_{i=1}^{k-1} \sum_{j=2}^{k} \beta_{ij} x_i x_j + \varepsilon \quad (1)$$

Table 1
Coded and actual levels of variables considered for matrix of variables for solution pH and accumulation time variable. Central composite face centered design for pH of DNOC solution values, time deposition, and obtained responses.

Variables	Symbol	Coded levels		
		−1	0	1
Accumulation time (s)	A	0	120	240
pH of DNOC solution	B	2	4.5	7

Run	Variables		Peak 1		Peak 2	
	A	B	i_p[a] (A)	E_p[b] (V)	i_p[a] (A)	E_p[b] (V)
1	120	7.0	-1.08×10^{-5}	−0.588	-1.00×10^{-5}	−0.763
2	240	2.0	-2.66×10^{-5}	−0.356	-2.47×10^{-5}	−0.515
3	0	7.0	-1.01×10^{-5}	−0.588	-9.13×10^{-6}	−0.763
4	120	4.5	-2.39×10^{-5}	−0.498	-2.33×10^{-5}	−0.704
5	240	4.5	-2.29×10^{-5}	−0.498	-2.21×10^{-5}	−0.704
6	120	4.5	-1.99×10^{-5}	−0.506	-1.88×10^{-5}	−0.728
7	0	4.5	-1.70×10^{-5}	−0.462	-1.57×10^{-5}	−0.656
8	0	2.0	-2.12×10^{-5}	−0.372	-1.95×10^{-5}	−0.531
9	240	7.0	-1.03×10^{-5}	−0.596	-9.62×10^{-6}	−0.763
10	120	4.5	-2.34×10^{-5}	−0.498	-2.24×10^{-5}	−0.720
11	120	2.0	-2.45×10^{-5}	−0.380	-2.23×10^{-5}	−0.539

[a] Peak current.
[b] Peak potential.

Table 2
Coded and actual levels of variables considered for matrix of variables for SWV. Box-Behnken design for instrumental variables and obtained responses.

Variables	Symbol	Coded levels		
		−1	0	1
Frequency	C	10	65	120
Amplitude	D	0.05	0.075	0.1
Step	E	0.005	0.0075	0.01

Run	Variables			Peak 1		Peak 2	
	C	D	E	i_p[a] (A)	SD[b] ip	i_p[a] (A)	SD[b] ip
1	10	0.05	0.0075	-8.62×10^{-6}	1.55×10^{-7}	-8.00×10^{-5}	1.48×10^{-7}
2	10	0.075	0.005	-1.04×10^{-5}	6.70×10^{-8}	-1.01×10^{-5}	2.87×10^{-7}
3	10	0.075	0.01	-2.22×10^{-5}	3.48×10^{-7}	-2.09×10^{-5}	4.32×10^{-7}
4	65	0.075	0.0075	-4.59×10^{-5}	1.36×10^{-6}	-4.38×10^{-5}	5.30×10^{-7}
5	120	0.05	0.0075	-4.25×10^{-5}	1.02×10^{-6}	-3.04×10^{-5}	7.73×10^{-7}
6	65	0.1	0.01	-5.45×10^{-5}	1.92×10^{-6}	-5.60×10^{-5}	1.38×10^{-6}
7	120	0.1	0.0075	-5.95×10^{-5}	1.08×10^{-6}	-5.41×10^{-5}	6.55×10^{-7}
8	65	0.075	0.0075	-5.05×10^{-5}	1.89×10^{-6}	-5.14×10^{-5}	1.73×10^{-6}
9	10	0.1	0.0075	-1.36×10^{-5}	1.36×10^{-7}	-1.24×10^{-5}	1.56×10^{-7}
10	120	0.075	0.005	-4.04×10^{-5}	1.55×10^{-6}	-3.39×10^{-5}	2.18×10^{-6}
11	65	0.075	0.0075	-4.67×10^{-5}	1.23×10^{-6}	-4.66×10^{-5}	1.50×10^{-6}
12	65	0.05	0.005	-3.13×10^{-5}	6.91×10^{-8}	-2.53×10^{-5}	5.93×10^{-7}
13	65	0.05	0.01	-3.42×10^{-5}	1.19×10^{-6}	-2.87×10^{-5}	1.25×10^{-6}
14	65	0.075	0.0075	-5.54×10^{-5}	7.31×10^{-7}	-5.36×10^{-5}	7.90×10^{-7}
15	65	0.1	0.005	-3.35×10^{-5}	8.11×10^{-7}	-3.30×10^{-5}	1.28×10^{-6}
16	65	0.075	0.0075	-4.02×10^{-5}	9.69×10^{-6}	-3.46×10^{-5}	9.55×10^{-6}
17	120	0.075	0.01	-5.33×10^{-5}	2.04×10^{-6}	-4.51×10^{-5}	1.58×10^{-6}

[a] Peak current.
[b] Standard deviation.

where Y is the predicted response, β_0 the offset term, β_i the coefficient of linear effect, β_{ii} the coefficient of squared effect, β_{ij} the coefficient of interaction effect, and ε the random error.

In this study, optimization process of solution pH and DNOC accumulation time for CSSWV determination was carried out using CCD, a total of 11 experiments were performed consisting of 3 factorial points (coded to the usual ± 1 notation), and 3 replicates at the centre points (0, 0, 0) in order to allow the estimation of pure error (Table 1). While BBD for SWV instrumental variables optimization, consisting of 12 factorial points and 5 replicates at the centre points in order to allow the estimation of pure error was used (Table 2), indicating that altogether 17 experiments were required.

2.7. Desirability function

The Derringer function (desirability function, DF) is the most currently used methodology to find optimal compromises between the total numbers of responses taken into account [31]. We have already used this function to obtain optimal conditions in other systems [32,33] where it was described. Basically, it establishes the relationship between the predicted responses on dependent variables and the desirability of the responses. Each estimated response variable was transformed into a dimensionless individual desirability value (di) using

the DF of the statistical program. First, the response is converted into a particular desirability function that varies from 0 to 1. The desirability 1 is for maximum while desirability 0 is for non-desirable situations or minimum. Inspecting the desirability profile, it determines which levels of the predictor variables produce the most desirable predicted response on the dependent variables [31].

3. Results and discussion

3.1. Comparison between GCE and SbFE

Nitro group can be electrochemical reduced by the generalized mechanism in a four electrons and four protons process to hydroxylamine in two steps:

$$R-NO_2 + e- \rightarrow R-NO_2^- \text{ (slow)}$$

$$R-NO_2- + 3\,e- + 4H^+ \rightarrow R-NHOH + H_2O \text{ (fast)}$$

As already mentioned, DNOC presents two nitro groups that are reduced at different potential values, so two differentiable cathodic current peaks are obtained. The electrochemical behaviour of 1×10^{-5} mol L^{-1} DNOC with glassy carbon electrode and SbFE is presented in Fig. 1. Results were obtained in BRBS pH 2 by CSSWV with an accumulation step at −0.16 V for 240 s under stirring and with the following SWV parameters, frequency 120 Hz, amplitude 0.10 V, and step potential −0.010 V. As it can be seen, at both electrodes two cathodic peaks corresponding to both nitro groups reduction are observed (peak 1 and peak 2). However, there are some remarkable differences on the voltammograms as the SWV profile for the SbFE modified electrode presents sharper peaks at lower potential values. Therefore, these results suggest that the SbFE is better suitable for determining DNOC when compared to unmodified GCE.

3.2. Optimization of DNOC determination by experimental design

3.2.1. CCD analysis design, optimization and validation of pH and accumulation time

The proposed mechanism for nitro group reduction involves four protons, so an SWV profile depending on pH is expected. Furthermore, DNOC has a pKa value of 4.48 [30], indicating that at lower pH values (2.50) the molecule would have no charge while for higher pH values (6.50) it will be negatively charged. For that reason solution pH was optimized together with the accumulation time by CCD using the reduction current peaks as dependant variables. As mentioned before, there is a pH current peak shift, for that reason the accumulation potential (E_{aa}) was not considered as a variable to optimize and fixed E_{aa} were employed for different pH values (−0.16 V, −0.26 V and −0.39 V for pH 2.0, 4.5, and 7.0, respectively). The design explains the significance and interaction effects of independent variables on the cathodic current and potential peaks; considering current peaks maximization. All the values reported correspond to an average of three samples analysis with the same antimony film (n = 3).

Table 1 presents DNOC reduction current (i_p) and potential (E_p) peaks (1 and 2) values after blank correction, for each CCD run, in 0.12 mol L^{-1} BRBS.

Fig. 2 presents SW voltammograms corresponding to Table 1 matrix runs. As expected, considering the reduction mechanism an important potential shift is observed for the reduction signals at different pH values. At more acidic pH, the current peaks appear at lower potential values while at pH 7.0 the lowest current peaks are observed. When considering the accumulation time, the most important effects is obtained for pH 2.0 where there is a continuous current increase with increasing accumulation time.

A mathematical model can be build up with all the analytical results by adjusting a second order polynomial function by minimum squared methodology. The ANOVA test was used to establish the significance of the multiple regression adjustment, and the lack of fit (LOF) for a 0.05 significance level. Table 3 summarizes the significant terms for the current (i_p) and potential (E_p) peaks together with the R-Squared (R^2), the model adjusted R-Squared (R^2_{adj}), predicted R-Squared (R^2_{pred}), p-values for LOF and the semi-empirical expressions for the fitted model equations. As it can be observed, both cathodic peaks can be modelled with the same significant terms. For the current peaks the two variables studied, accumulation time (A) and solution pH (B) either in the lineal (A and B) and the quadratic terms (A^2 and B^2) and the interaction (A–B) must be included in the model. On the other side, for both peaks potential, the lineal and the quadratic terms are significant. The LOF p-values indicate that the analysis is not significant with respect to the pure error ($p > 0.05$). Furthermore, the R-squared values ($R^2_{adj} > 0.893$ and $R^2_{pred} > 0.752$) demonstrate that >89.3% of the model variability and >75.2% of new data variability can be satisfactorily explained by the models. In all cases, both values corresponds each other, as the difference between them is <0.2 indicating a

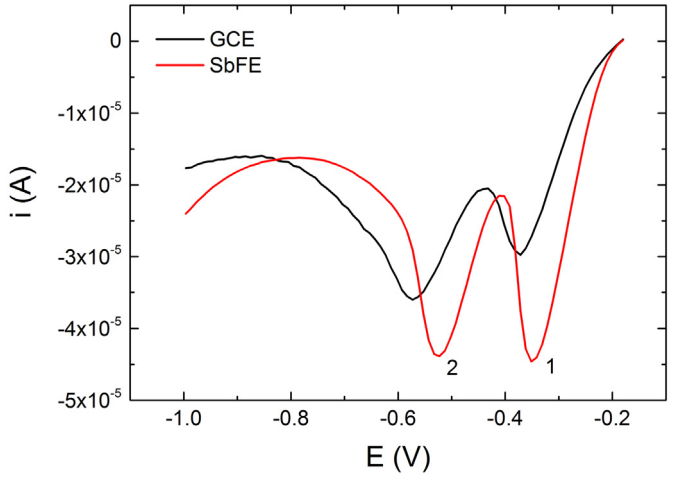

Fig. 1. Square wave voltammograms of 1×10^{-5} mol L^{-1} DNOC in BRBS pH 2 at (black) GCE and (red) SbFE. E_{acc} −0.16 V, t_{acc} 240 s, 120 Hz frequency, 0.10 V amplitude, and 0.01 V step. (For interpretation of the references to color in this figure legend, the reader is referred to the web version of this article.)

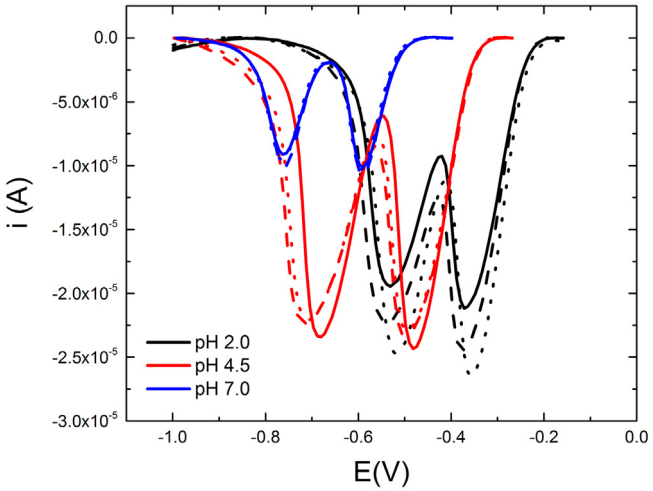

Fig. 2. Square wave voltammograms of 1×10^{-5} mol L^{-1} DNOC at SbFE electrode in 0.12 mol L^{-1} BRBS at different pH values 2.0 (black); 4.5 (red), and 7 (blue) at three accumulation time values 0 s (solid), 120 s (dash), and 240 s (dot). SWV parameters: 45 Hz frequency, 0.02 V amplitude, and 0.008 V step. E_{acc} −0.16 V, −0.26 V, and −0.39 V for pH 2.0, 4.5, and 7.0, respectively. (For interpretation of the references to color in this figure legend, the reader is referred to the web version of this article.)

Table 3
Significant terms and statistics summary of response surface models for pH (A) and accumulation time (B) optimizations.

	Significant terms	R^2	R^2_{adj}	R^2_{pred}	LOF	Fitted model
Peak 1						
Current peak (A)	A, B, AB, A^2 and B^2	0.960	0.921	0.826	0.790	$i_p = -1.63 \times 10^{-5} - 5.98 \times 10^{-8}\,A - 3.22 \times 10^{-6}\,B + 4.30 \times 10^{-9}\,AB + 1.02 \times 10^{-10}\,A^2 + 6.05 \times 10^{-7}\,B^2$
Potential peak (V)	A, B, A^2 and B^2	0.987	0.978	0.945	0.0837	$E_p = -0.25 - 2.54 \times 10^{-4}\,A - 0.06\,B + 8.95 \times 10^{-7}\,A^2 + 1.40 \times 10^{-3}\,B^2$
Peak 2						
Current peak (A)	A, B, AB, A^2 and B^2	0.947	0.893	0.752	0.754	$i_p = -1.31 \times 10^{-5} - 5.93 \times 10^{-8}\,A - 3.98 \times 10^{-6}\,B + 3.97 \times 10^{-9}\,AB + 1.02 \times 10^{-10}\,A^2 + 6.68 \times 10^{-7}\,B^2$
Potential peak (V)	A, B, A^2 and B^2	0.978	0.964	0.916	0.263	$E_p = -0.31 - 4.13 \times 10^{-4}\,A - 0.12\,B + 1.53 \times 10^{-6}\,A^2 + 8.17 \times 10^{-3}\,B^2$

reasonable agreement. Different diagnosis graphs were also evaluated, among them normal probability distributions, studentised vs. predicted, external studentised residuals, leverage DFFITS, DFBETAS and Cook distance, demonstrating that the model satisfactorily explain the experimental results (not shown).

The 3D response surface plots were obtained (Fig. 3) for peak 1 current (Fig. 3 A) and potential (Fig. 3 B) values, to determine the dependence of dependent variables on independent ones. The response presented in Fig. 3 A shows a maximum (in absolute values) at pH 2 and at the highest accumulation time, the effect of both quadratic terms can also be observed in the figure and explains the current peaks values obtained without accumulation time. On the other side, Fig. 3 B presents the dependence of peak 1 potential with the two independent variables were the lowest potential values are obtained for pH 2.0. Both results are in agreement with SWV voltammograms presented in Fig. 2.

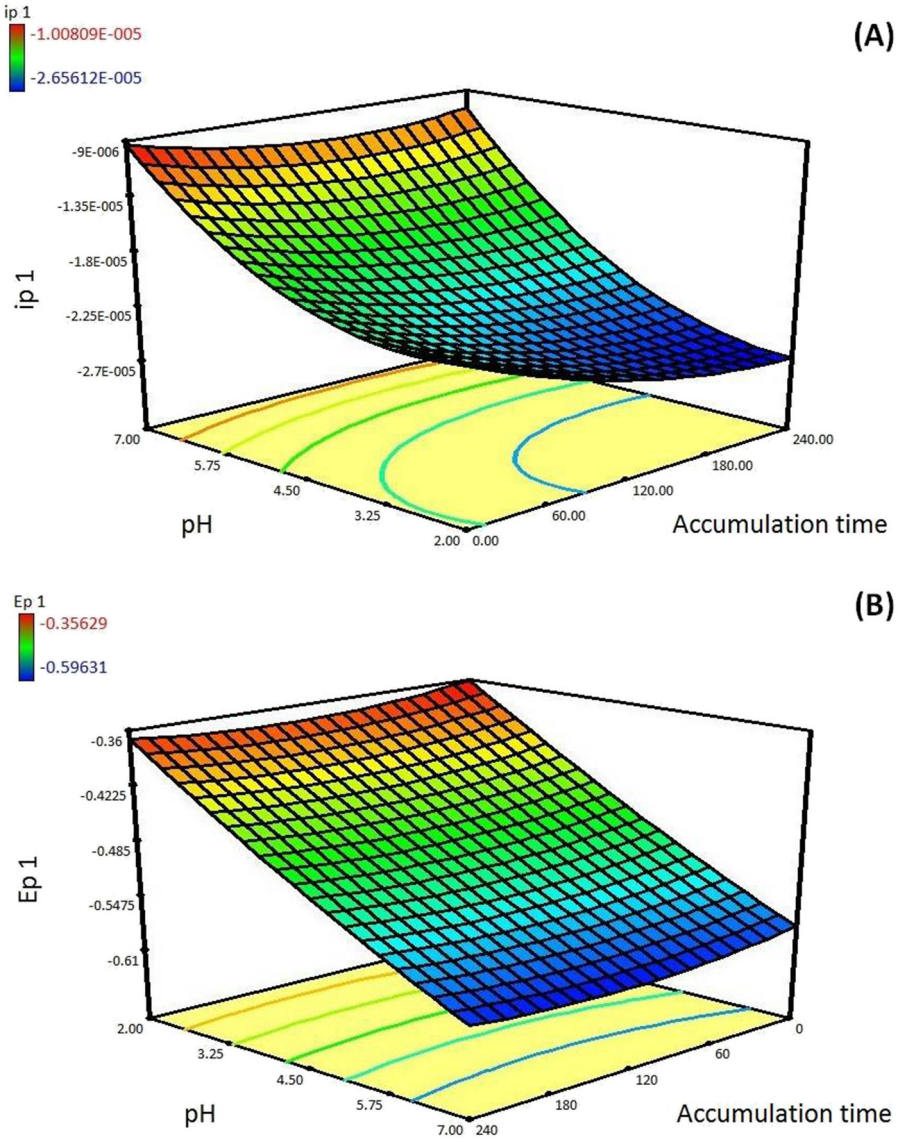

Fig. 3. Response surface for peak 1 results current (A) and potential (B) for the CCD data in Table 1.

As already described in Section 2.7 profiling the desirability of responses involves specifying the DF for the dependent variable (i_p), by assigning predicted values in a scale ranging from 0.0 (undesirable) to 1.0 (very desirable), to reach this purpose, current peak values were maximized (in absolute value) with a +++++ (5 of 5) significance for both peak values. On the basis of these calculations and desirability score of 1.000, i_p for DNOC reduction was optimized at (27 ± 5) μA and (25 ± 6) μA with a 95% of confidence for peak 1 and 2, respectively. This current value was calculated according to the proposed model with the following conditions: pH 2.3 and 214 s accumulation time. Confirmation of the optimized conditions validation was carried on by experimental results (triplicate) that were then compared to predicted values. The reduction current peak of 1×10^{-5} mol L^{-1} DNOC using these optimum conditions was found to be (24.9 ± 0.1) μA for peak 1 and (25 ± 1) μA for peak 2. The mean value obtained was compared with the predicted value indicating the suitability of the developed quadratic model.

3.2.2. BBD analysis design, optimization, and validation of the SWV instrumental variables

DNOC quantification was performed with a SbFE modified glassy carbon electrode by SWV using an accumulation step previously optimized at −0.16 V for 214 s in BRBS pH 2.3. Under the optimized DNOC accumulation conditions, SWV variables such as frequency, amplitude and step potential were also optimized. In this case there are three independent factors and the reduction current peaks and their corresponding standard deviations are used as response variables, so a BBD was chosen. Table 2 presents the BBD matrix along with experimental data obtained in 0.12 mol L^{-1} BRBS pH = 2.3. The instrumental variables analysed were frequency (C), amplitude (D), and step potential (E). Again an ANOVA test was performed and the significant results are summarized in Table 4. All the instrumental variables are significant either in their linear or quadratic form for all the four dependent variables. On the other side, interactions between C–D and D–E are also significant for all the variables except for peak 2 current value standard deviation. As already mentioned for the CCD, also for the BBD design the LOF p-values indicate that the analysis is not significant with respect to the pure error in all cases ($p > 0.05$). Furthermore, the R-squared values for both i_p, summarized in Table 4 demonstrate that >86.7% of the model variability and >80.0% of new data variability can be satisfactorily explained by the current peak models. In both cases, values corresponds each other, as the difference between them is <0.2 indicating a reasonable agreement. In the SD case, data were transformed to 1.0/Sqrt and the R-square values were >0.862 (R^2), >0.779 (R^2_{adj}) and >0.621 (R^2_{pred}), as in the previous case the difference between the last two values is <0.2. However, although in the case of SD >86.2% of the observed variability is explained by the model while 77.9% of new data variability can be explained by the model, results for this analysis are considered satisfactory.

The significant effects for current peak 1 versus the significant variables are displayed in Fig. 4, where a 3D representation of the polynomial equation (Table 4) obtained from the experimental data is presented. The variation of i_{p1} as a function of two independent variables while the third remains constant is presented in Fig. 4. Fig. 4 A shows i_{p1} versus amplitude and frequency at a 0.0075 V step, Fig. 4 B shows the variation of i_{p1} with step and frequency at a 0.075 V amplitude and finally in Fig. 4 C the dependence of i_{p1} on the step and amplitude at a 65 Hz frequency is shown. As it can be observed, in all cases maximum current peaks (in absolute value) are obtained for the highest independent variables values. A similar behaviour is observed for i_{p2} (not shown).

In Fig. 5, the 2D amplitude-frequency contour plot of the standard deviation for both current peaks at low, medium and high step potential values are presented. As it can be observed, the current peak 1 standard deviation presents the lowest values in the whole frequency range for medium to low amplitude values and low step potential (Fig. 5 A), also for low amplitude values when the step potential is medium (Fig. 5B) and for high amplitude values at high step potential (Fig. 5C). For the other side, current peak 2 standard deviation presents minimum values at low frequency for all the amplitude values for the three step potential levels.

In order to obtain the best operational conditions and as already described for CCD, the DF was used to maximize absolute current peaks values and to minimize both SD values for the three independent variables. To reach this purpose, current peak values were maximized with a +++++ (5 of 5) significance while the SD for the triplicate signals for each new SbFE was minimized with a ++ (2 of 5) significance and three different optimal solutions were obtained (Table 5). It is worthy to note that solution 1 corresponds to all the variables in their highest values while for solution 3 all the variables are at their middle values, these results agree with the behaviour already described for SD_{ip1} (Fig. 5). Fig. 6 presents the DF for the amplitude-frequency at the three step potential values levels. In agreement with already discussed results (Figs. 4 and 5 and Table 5), a maximum DF value is obtained when instrumental variables are at the highest values (Fig. 6C). Experiments using the conditions obtained by the different solutions were carried on to choose the best one and the obtained results indicate that the highest current values were obtained for solution 1 while the SD values were similar for all three solutions. For that reason, solution 1 (120 Hz frequency, 0.10 V amplitude and 0.01 V step) was chosen as the optimum operational condition. To confirm the validity of the model; experiments were carried out to compare experimental results with predicted values using the model equation. DNOC reduction current peaks were found to be −63.2 μA and −59.1 μA with a 95% prediction interval between −48.0 μA and −78.4 μA and −40.2 μA and −77.9 μA for peak 1 and 2, respectively. On the other side, experimental values obtained with three different SbFEs for 1×10^{-5} mol L^{-1} DNOC were −57.1 ± 0.5 μA and −51.1 ± 0.5 μA for peak 1 and 2, respectively. Obtained mean values were compared with predicted ones indicating the suitability of the developed quadratic model.

Table 4
Significant terms and statistics summary of response surface models for SWV optimizations.

	Significant terms	R^2	R^2_{adj}	R^2_{pred}	LOF	Fitted model
Peak 1						
Cathodic current peak	C, D, E, CD, DE, C^2, D^2 y E^2	0.959	0.917	0.847	0.839	$i\,(A) = -5.70 \times 10^{-5} - 6.61 \times 10^{-7} C - 7.18 \times 10^{-4} D - 7.59 \times 10^{-3} E - 2.18 \times 10^{-6} CD - 0.07\,DE + 3.88 \times 10^{-8} C^2 + 7.90 \times 10^{-7} D^2 + 0.71\,E^2$
1.0/Sqrt (Standard Deviation i_p)	C, D, E, CD, DE, C^2, D^2 y E^2	0.909	0.818	0.621	0.125	$1/(SD)^{1/2} = 2.08 \times 10^4 - 69.19C - 1.94 \times 10^5 D - 2.24 \times 10^6 E + 3.76 \times 10^4 CD + 1.00 \times 10^7 DE + 0.19\,C^2 + 7.01 \times 10^5 D^2 + 6.48 \times 10^7 E^2$
Peak 2						
Cathodic current peak	C, D, E, CD, DE, C^2, D^2 y E^2	0.933	0.867	0.800	0.936	$i\,(A) = 6.27 \times 10^{-5} - 5.93 \times 10^{-7} C - 8.83 \times 10^{-4} D - 7.22 \times 10^{-3} E - 3.51 \times 10^{-6} CD - 0.08\,DE + 4.63 \times 10^{-9} C^2 + 9.24 \times 10^{-3} D^2 + 0.71\,E^2$
1.0/Sqrt (Standard Deviation i_p)	C, D, E, C^2, D^2 y E^2	0.862	0.779	0.698	0.945	$1/(SD)^{1/2} = 3.75 \times 10^4 - 37.04C - 9.36 \times 10^5 D + 6.37 \times 10^6 E + 0.20\,C^2 + 6.09 \times 10^5 D^2 - 4.47 \times 10^7 E^2$

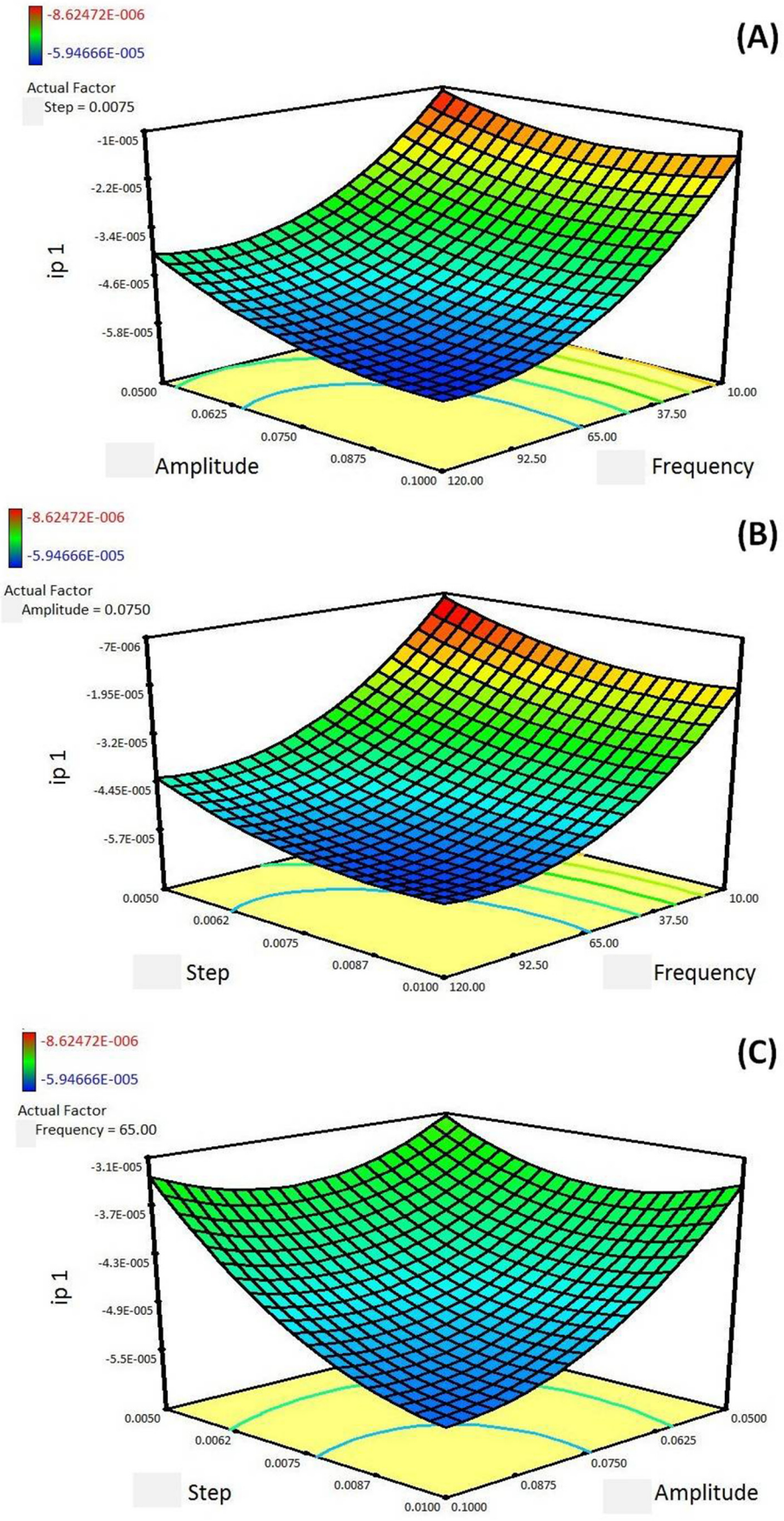

Fig. 4. Response surface of the current peak 1 for the Box Behnken designs of data in Table 2: (A) Amplitude (V)–Frequency (Hz), (B) Step (V)–Frequency (Hz) and (C) Step (V)– Amplitude (V).

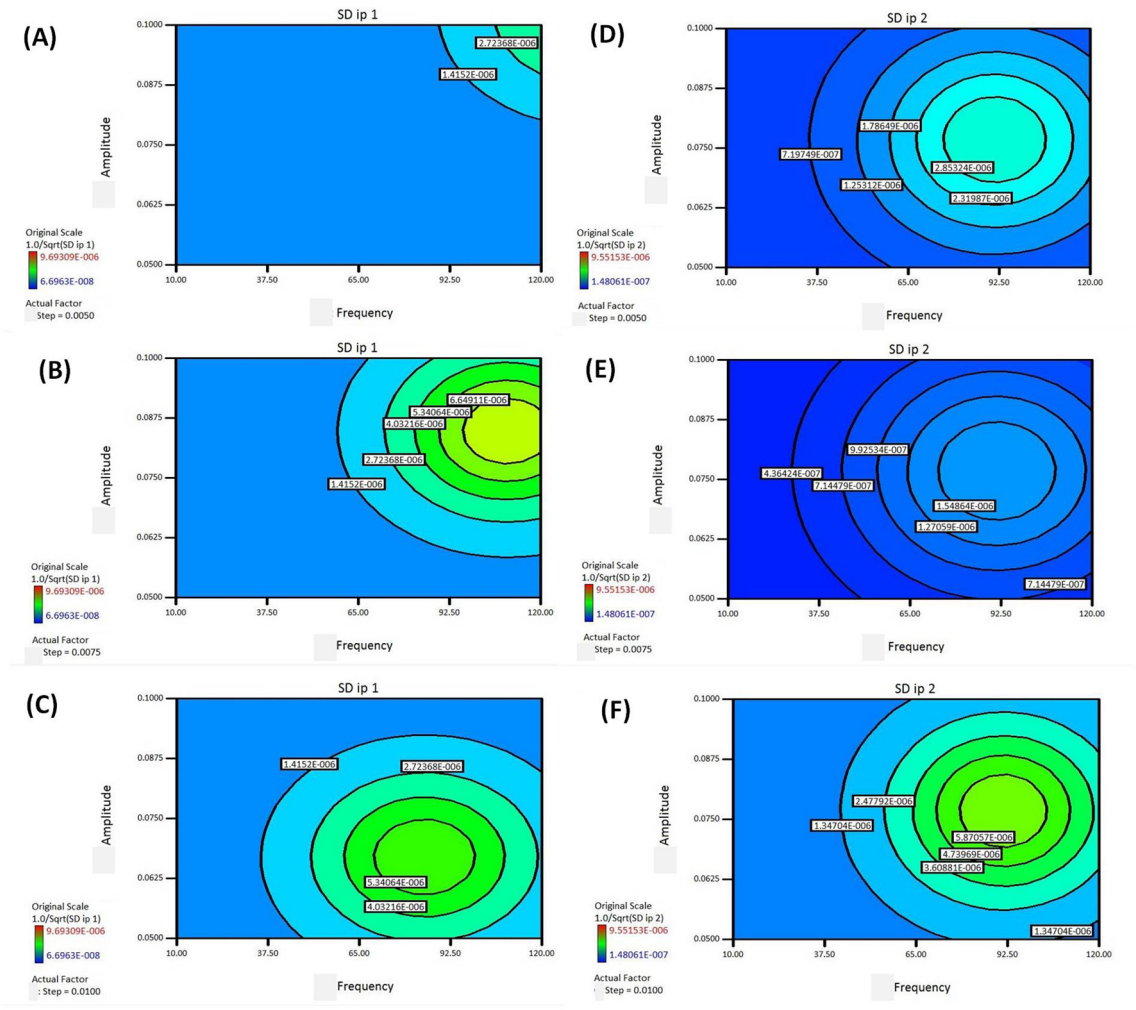

Fig. 5. 2D Amplitude-Frequency contour plot of the current peak standard deviation for the Box Behnken of data in Table 2: (A, B and C) peak 1, (D, E and F) peak 2 for (A and D) step 0.005, (B and E) step 0.075 and (C and F) step 0.01.

3.3. Method performance

3.3.1. Linearity and related figures of merit

Due to the fact that both current peaks have a similar behaviour, the analytical method was tested only with peak 1 current as it is the one that show higher current values. To check the method linearity, triplicate measurements at five concentration levels were performed under the analytical procedure in the (1.0–15.0) $\times$ 10^{-6} mol L^{-1} DNOC concentration range. Calibration curves were fitted by least-squares and R^2 value >0.999 were obtained. The limit of detection (LOD) and quantification (LOQ) was calculated on the basis of the residual standard deviation ($S_{y/x}$) and the slope (S) of the calibration curves

Table 5
Upper and lower limits that were chosen for the responses and factors to instrumental SWV optimization and possible solutions in order of desirability.

Constraints				
		Lower	Upper	
Name	Goal	Limit	Limit	Importance
Frequency	Is in range	10	120	3
Amplitude	Is in range	0.05	0.1	3
Step	Is in range	0.005	0.01	3
i_{p1} (A)	Minimize	-5.95×10^{-5}	-8.62×10^{-6}	5
SD i_{p1}	Minimize	6.70×10^{-8}	9.69×10^{-6}	2
i_{p2} (A)	Minimize	-5.60×10^{-5}	-7.80×10^{-6}	5
SD i_{p2}	Minimize	1.48×10^{-7}	9.55×10^{-6}	2

Solutions				
Optimo number	Frequency	Amplitude	Step	Desirability
1	120.0	0.10	0.0100	0.689
2	70.3	0.10	0.0097	0.641
3	70.7	0.062	0.0066	0.526

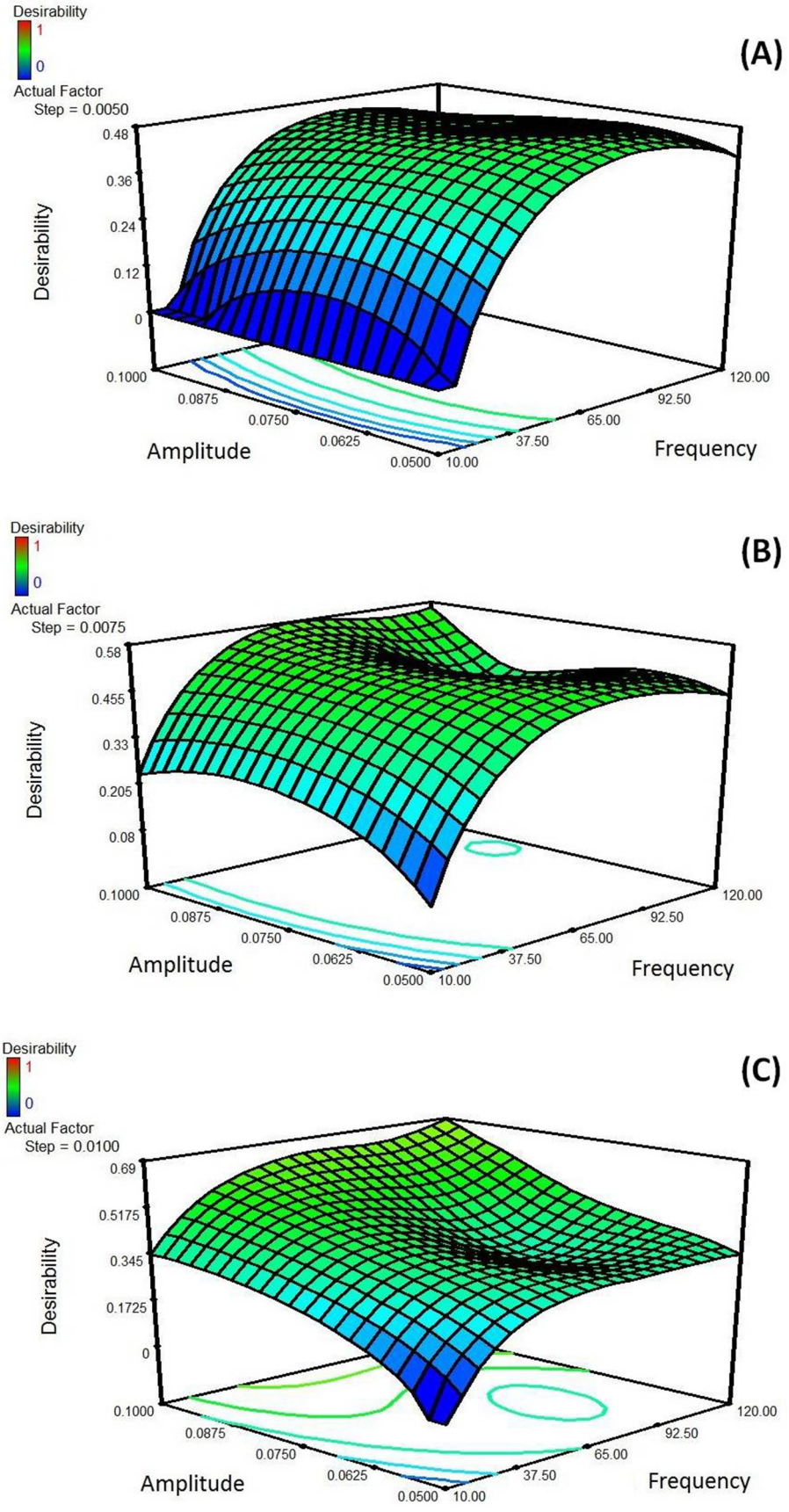

Fig. 6. Response surface of the Amplitude (V)–Frequency (Hz) desirability function for the Box Behnken designs of data in Table 2: (A) Step 0.005 V, (B) Step 0.0075 V and (C) Step 0.010 V.

Table 6
Analysis of known concentration solutions and natural water samples.

Theoretical ($\times 10^{-6}$ mol L^{-1})	Experimental ($\times 10^{-6}$ mol L^{-1}) ± SD[a]	CV[b] (%)	p-Value
1	1.0 ± 0.1	10	0.806
5	5.0 ± 0.6	11	0.9745
10	9.9 ± 0.7	7	0.784

Sample N°	Added ($\times 10^{-6}$ mol L^{-1})	Found ($\times 10^{-6}$ mol L^{-1})[c]	Recovery (%) ± SD[a]
Rio Tercero	5	5.32	106 ± 3
Lago San Roque	5	5.22	104 ± 2
Canilla	5	4.73	95 ± 4

[a] Mean values and standard deviation of three determinations.
[b] CV: coefficient of variation.
[c] SWV measurements were repeated five times (n = 3).

at the levels approaching the limits according to the equation LOD = 3.3 ($S_{y/x}$/S) and LOQ = 10($S_{y/x}$/S) [38]. The following values were found: LOD 1.12×10^{-6} mol L^{-1} and LOQ 1.42×10^{-6} mol L^{-1}.The final calibration equation calculated by the average and standard deviation for the slope and the intercept of all the calibration curves is:

$$i_{p1}(A) = (-6.9 \pm 0.9) \times 10^{-6} + (-4.8 \pm 0.2)\, C_{DNOC}\left(Amol^{-1}L^{-1}\right)$$

3.3.2. Precision

The intra-assay precision studies (repeatability) were carried out using three replicate samples at three levels of concentration (1×10^{-6}, 5×10^{-6}, and 10×10^{-6} mol L^{-1}), under the same conditions and on the same day. Table 6 shows the coefficient of variation (CV %) values for different DNOC concentrations and results for current peak values at intermediate precision under different conditions. As it can be observed, CV values near 10% are obtained, indicating a good precision for the present method.

3.3.3. Accuracy

The accuracy was obtained by measuring known concentration samples and comparing the experimental concentration to the true value at three levels. In Table 6 theoretical and the obtained averages concentration values, together with Student's *t*-test p values are presented. The Student's t-test that compare both concentration values establishes that there are no statistical differences at 95% confidence level between the results achieved by the three concentration values.

3.3.4. Application to real sample analysis

Finally, the proposed analytical method was tested for DNOC detection in water samples to validate the potential application in real analysis. Water samples were prepared according to Section 2.2, and experiments were performed by the standard addition method. In Table 6 added and found DNOC concentration, together with SD and recovery % are presented. It can be observed that in all cases satisfactory recovery results are obtained the average recovery value being 102%, confirming the validity of the developed method.

4. Conclusion

A validated method for DNOC determination in water samples has been developed. An antimony film electrode has been used coupled to cathodic stripping square wave voltammetry. The solution pH and the accumulation time together with SWV instrumental parameter were optimized with a CCD and BBD combining RSM and DF respectively, to obtain the optimal conditions for the highest reduction current peak. Optimal conditions for the analytical method involve an accumulation step at pH 2.30 for 214 s, while DNOC quantifications was performed by striping SWV at 120 Hz frequency, 0.10 V amplitude, and 0.01 V step potential. Based on these results, a linear calibration curve ranged from $(1.0 \text{ to } 15) \times 10^{-6}$ mol L^{-1} with a detection limit of 1.12×10^{-6} mol L^{-1} was obtained. Finally, the method has been successfully applied to DNOC detection in natural water samples.

Acknowledgments

The authors wish to acknowledge the assistance of CONICET (PIP 112-201101-00579), UNC (project resolution 113/17) and FONCyT (PICT 12/0634), whose support facilities and funds were used in this investigation. J.M.B. and M.C. acknowledge a doctoral fellowship from CONICET. P.O. and V.P. are members of CICyT CONICET, the National Science Foundation of Argentina.

References

[1] C.M. Brett, A.M. Brett, Electrochemistry: Principles, Methods, and Applications, Oxford University Press Inc., New York, 1993.
[2] S.B. Hocevar, I. Svancara, B. Ogorevc, K. Vytras, Antimony film electrode for electrochemical stripping analysis, Anal. Chem. 79 (2007) 8639–8643, https://doi.org/10.1021/ac070478m.
[3] N. Serrano, J.M. Díaz-Cruz, C. Ariño, M. Esteban, Antimony-based electrodes for analytical determinations, TrAC Trends Anal. Chem. 77 (2016) 203–213, https://doi.org/10.1016/j.trac.2016.01.011.
[4] C. Pérez-Ràfols, P. Trechera, N. Serrano, J.M. Díaz-Cruz, C. Ariño, M. Esteban, Determination of Pd(II) using an antimony film coated on a screen-printed electrode by adsorptive stripping voltammetry, Talanta 167 (2017) 1–7, https://doi.org/10.1016/j.talanta.2017.01.084.
[5] S. Dal Borgo, V. Jovanovski, S.B. Hocevar, Antimony film electrode for stripping voltammetric measurement of Hg(II) in the presence of Cu(II), Electrochim. Acta 88 (2013) 713–717, https://doi.org/10.1016/j.electacta.2012.10.122.
[6] A. Bobrowski, M. Putek, J. Zarebski, Antimony film electrode prepared in situ in hydrogen potassium tartrate in anodic stripping voltammetric trace detection of Cd (II), Pb(II), Zn(II), Tl(I), In(III) and Cu(II), Electroanalysis 24 (2012) 1071–1078, https://doi.org/10.1002/elan.201200015.
[7] V. Sosa, C. Barceló, N. Serrano, C. Ariño, J.M. Díaz-Cruz, M. Esteban, Antimony film screen-printed carbon electrode for stripping analysis of Cd(II), Pb(II), and Cu(II) in natural samples, Anal. Chim. Acta 855 (2015) 34–40, https://doi.org/10.1016/j.aca.2014.12.011.
[8] M. Frena, I. Campestrini, O.C. de Braga, A. Spinelli, In situ bismuth-film electrode for square-wave anodic stripping voltammetric determination of tin in biodiesel, Electrochim. Acta 56 (2011) 4678–4684, https://doi.org/10.1016/j.electacta.2011.02.111.
[9] V. Guzsvány, H. Nakajima, N. Soh, K. Nakano, T. Imato, Antimony-film electrode for the determination of trace metals by sequential-injection analysis/anodic stripping voltammetry, Anal. Chim. Acta 658 (2010) 12–17, https://doi.org/10.1016/j.aca.2009.10.049.
[10] C. Kokkinos, A. Economou, Disposable microfabricated 3-electrode electrochemical devices with integrated antimony working electrode for stripping voltammetric determination of selected trace metals, Sensors Actuators B Chem. 192 (2014) 572–577, https://doi.org/10.1016/j.snb.2013.11.040.
[11] M.K. Dey, A.K. Satpati, A.V.R. Reddy, Electrodeposited antimony and antimony–gold nanocomposite modified carbon paste electrodes for the determination of heavy metal ions, Anal. Methods 6 (2014) 5207, https://doi.org/10.1039/c4ay00876f.
[12] V. Jovanovski, S.B. Hočevar, B. Ogorevc, Ex situ prepared antimony film electrode for electrochemical stripping measurement of heavy metal ions, Electroanalysis 21 (2009) 2321–2324, https://doi.org/10.1002/elan.200904692.
[13] C. Barceló, N. Serrano, C. Ariño, J.M. Díaz-Cruz, M. Esteban, Ex-situ antimony screen-printed carbon electrode for voltammetric determination of Ni(II)-ions in wastewater, Electroanalysis 28 (2016) 640–644, https://doi.org/10.1002/elan.201500511.
[14] B. Sebez, B. Ogorevc, S.B. Hocevar, M. Veber, Functioning of antimony film electrode in acid media under cyclic and anodic stripping voltammetry conditions, Anal. Chim. Acta 785 (2013) 43–49, https://doi.org/10.1016/j.aca.2013.04.051.
[15] C. Kokkinos, A. Economou, I. Raptis, T. Speliotis, Novel disposable microfabricated antimony-film electrodes for adsorptive stripping analysis of trace Ni(II), Electrochem. Commun. 11 (2009) 250–253, https://doi.org/10.1016/j.elecom.2008.11.022.
[16] V. Urbanová, K. Vytřas, A. Kuhn, Macroporous antimony film electrodes for stripping analysis of trace heavy metals, Electrochem. Commun. 12 (2010) 114–117, https://doi.org/10.1016/j.elecom.2009.11.001.
[17] H. Sopha, V. Jovanovski, S.B. Hocevar, B. Ogorevc, In-situ plated antimony film electrode for adsorptive cathodic stripping voltammetric measurement of trace nickel, Electrochem. Commun. 20 (2012) 23–25, https://doi.org/10.1016/j.elecom.2012.03.048.
[18] C. Pérez-Ràfols, N. Serrano, J.M. Díaz-Cruz, C. Ariño, M. Esteban, New approaches to antimony film screen-printed electrodes using carbon-based nanomaterials substrates, Anal. Chim. Acta 916 (2016) 17–23, https://doi.org/10.1016/j.aca.2016.03.003.

[19] A.M. Ashrafi, K. Vytřas, New procedures for voltammetric determination of copper (II) using antimony film-coated carbon paste electrodes, Electrochim. Acta 73 (2012) 112–117, https://doi.org/10.1016/j.electacta.2011.12.042.
[20] C. Pérez-Ràfols, N. Serrano, J.M. Díaz-Cruz, C. Ariño, M. Esteban, Simultaneous determination of Tl(I) and In(III) using a voltammetric sensor array, Sensors Actuators B Chem. 245 (2017) 18–24, https://doi.org/10.1016/j.snb.2017.01.089.
[21] A.M. Ashrafi, K. Vytřas, Stripping voltammetric determination of mercury(II) at antimony-coated carbon paste electrode, Talanta 85 (2011) 2700–2702, https://doi.org/10.1016/j.talanta.2011.07.078.
[22] B. Nigović, S.B. Hocevar, Antimony film electrode for direct cathodic measurement of sulfasalazine, Electrochim. Acta 58 (2011) 523–527, https://doi.org/10.1016/j.electacta.2011.09.087.
[23] B. Nigović, S.B. Hocevar, Square-wave voltammetric determination of pantoprazole using exsitu plated antimony-film electrode, Electrochim. Acta 109 (2013) 818–822, https://doi.org/10.1016/j.electacta.2013.07.173.
[24] J.A. Rodríguez, M.G. Juárez, C.A. Galán-Vidal, J.M. Miranda, E. Barrado, Determination of allura red and tartrazine in food samples by sequential injection analysis combined with voltammetric detection at antimony film electrode, Electroanalysis 27 (2015) 2329–2334, https://doi.org/10.1002/elan.201500295.
[25] G. Krepper, G.D. Pierini, M.F. Pistonesi, M.S. Di Nezio, "In-situ" antimony film electrode for the determination of tetracyclines in Argentinean honey samples, Sensors Actuators B Chem. 241 (2017) 560–566, https://doi.org/10.1016/j.snb.2016.10.125.
[26] J. Gajdár, J. Barek, J. Fischer, Antimony film electrodes for voltammetric determination of pesticide trifluralin, J. Electroanal. Chem. 778 (2016) 1–6, https://doi.org/10.1016/j.jelechem.2016.08.011.
[27] E.A. Hutton, B. Ogorevc, M.R. Smyth, Cathodic electrochemical detection of nitrophenols at a bismuth film electrode for use in flow analysis, Electroanalysis 16 (2004) 1616–1621, https://doi.org/10.1002/elan.200402979.
[28] M. Marcel, J. Nunes, A. Spinelli, www.scielo.br/eq 36 (2) (2011) 158–181 2011, 36.
[29] M. Kotoucek, Voltammetric behaviour of some nitropesticides at the mercury drop electrode, Anal. Chim. Acta 329 (1996) 73–81, https://doi.org/10.1016/0003-2670(96)00133-X.
[30] A.F. Pelfrene, Dinitro-ortho-cresol, Environ. Health 220 (2000).
[31] D. Montgomery, Design and Analysis of Experiments, 3rd ed. John Wiley and Sons, New York, 1991http://www.philadelphia.edu.jo/math/syllabi/210331.pdf, Accessed date: 16 October 2013.
[32] M. Cuéllar, V. Pfaffen, P.I. Ortiz, Application of multi-factorial experimental design to successfully model and optimize inorganic chromium speciation by square wave voltammetry, J. Electroanal. Chem. 765 (2016) 37–44, https://doi.org/10.1016/j.jelechem.2015.07.050.
[33] G. Bia, L. Borgnino, P.I. Ortiz, V. Pfaffen, Multivariate optimization of square wave voltammetry using bismuth film electrode to determine atrazine, Sensors Actuators B Chem. 203 (2014)https://doi.org/10.1016/j.snb.2014.07.003.
[34] R.F. Teófilo, E.L. Reis, C. Reis, G.A. Silva, L.T. Kubota, Experimental design employed to square wave voltammetry response optimization for the glyphosate determination, J. Braz. Chem. Soc. 15 (2004) 865–871.
[35] G. Krepper, P.B. Resende de Cerqueira, M.F. Pistonesi, M.S. Di Nezio, M.E. Centurión, Determination of cadmium residues in bee products using a "lab-made" bismuth bulk electrode, Int. J. Environ. Anal. Chem. 96 (2016) 1331–1340, https://doi.org/10.1080/03067319.2016.1250893.
[36] G. Zhao, H. Wang, G. Liu, Z. Wang, Box-Behnken response surface design for the optimization of electrochemical detection of cadmium by Square Wave Anodic Stripping Voltammetry on bismuth film/glassy carbon electrode, Sensors Actuators B Chem. 235 (2016) 67–73, https://doi.org/10.1016/j.snb.2016.05.051.
[37] R. Leardi, Experimental design in chemistry: a tutorial, Anal. Chim. Acta 652 (2009) 161–172, https://doi.org/10.1016/j.aca.2009.06.015.
[38] J.N. Miller, J.C. Miller, Statistics and Chemometrics for Analytical Chemistry, Fifth Ellison Horwood, Chichester, 2005.